

Noise-induced stop-and-go traffic dynamics: Modelling and control

Raphael Korbmacher^a, Parthib Khound^b, Antoine Tordeux^{a,*}, and Frank Gronwald^c

^aUniversity of Wuppertal, Gaußstraße 20, 42119 Wuppertal, Germany

^bIndian Institute of Technology Bombay, 400076 Mumbai, India

^cUniversity of Siegen, Hölderlinstraße 3, 57076 Siegen, Germany

Keywords:

Road traffic flow

Stop-and-go wave

Noise-induced instability

Nonlinear instability

Stabilisation

This contribution investigates an original stochastic approach for the emergence of stop-and-go waves in traffic flow, a collective phenomenon with significant safety and environmental implications. Using a stable nonlinear car-following model, the study shows that minimal white Gaussian noise can destabilise the flow, leading to a phase transition from laminar to periodic dynamics through a nonlinear instability phenomenon, analogous to Kapitza's pendulum. Furthermore, a simple linear transformation of the model, which amplifies the response and introduces a positive acceleration bias, counteracts noise-induced effects and recovers the stability of uniform solutions. The findings are supported by simulations, offering new insights into the modelling and mitigation of oscillatory traffic dynamics.

1 Introduction

Most car drivers have experienced stop-and-go waves on highways where traffic jams emerge for no apparent reason, forcing drivers to repeatedly slow down and speed up. These waves are a fascinating collective phenomenon that can be observed worldwide. Beyond their scientific intrigue, stop-and-go dynamics pose significant safety risks and environmental challenges, as the constant acceleration and deceleration increase fuel consumption and pollutant emissions [36]. The terminology of *stop-and-go waves* can be traced back to Duckstein in the late 1960s [7], with related terms like *phantom jam* [53] or *jamiton* [10] describing their occurrence for no apparent reason. This phenomenon was empirically demonstrated in the late 2000s through an experiment with 22 vehicles on a single-lane circuit [53], as shown in Fig. 1. Starting from a homogeneous configuration with equal spacing, stop-and-go waves emerge after a while, resulting in self-sustained oscillatory dynamics.

Despite over seven decades of research on traffic instabilities and stop-and-go dynamics, the emergence of self-sustaining waves in traffic flow remains to be not completely understood. Recent experiments

* Corresponding author. E-mail address: tordeux@uni-wuppertal.de.

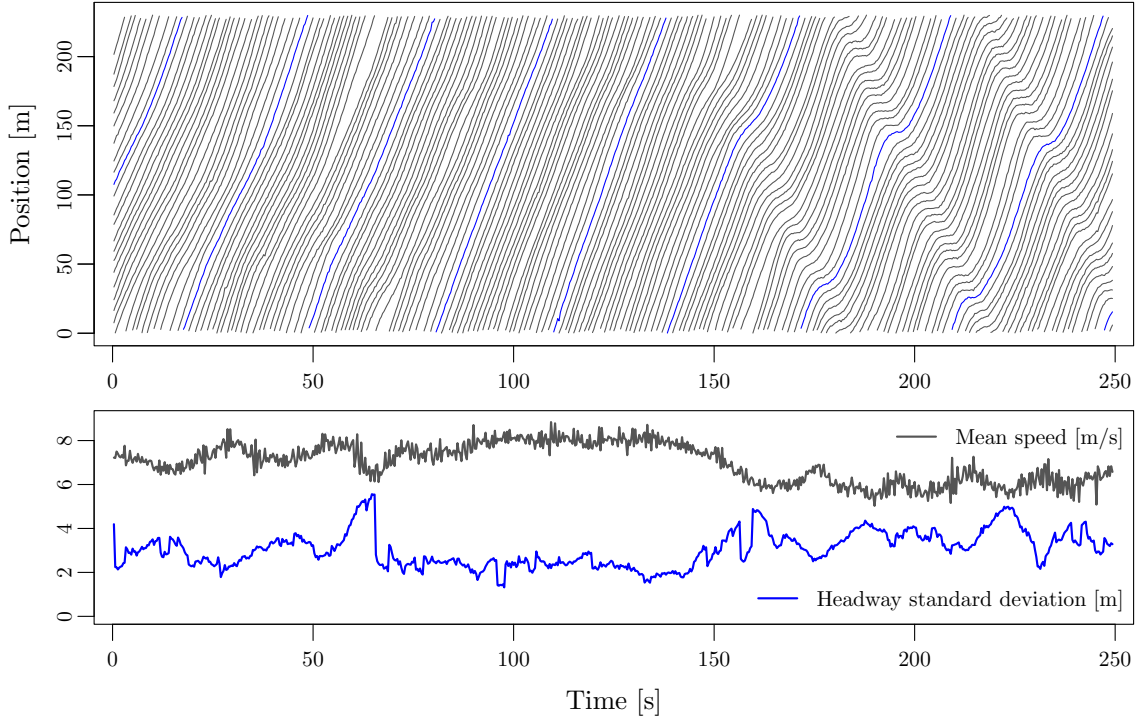


Figure 1: Experimental trajectories of 22 vehicles on a single-lane circuit starting from a uniform configuration [53]. After a while, a stop-and-go wave appears, causing the average speed to decrease and the standard deviation of the gap to increase.

reveal that even advanced driver assistance systems, such as adaptive cruise control (ACC), exhibit major stability issues [41, 18, 6, 35, 38]. Understanding and mitigating traffic oscillations remains a complex challenge, with ongoing efforts exploring novel approaches [31]. For instance, experiments with up to 100 autonomous vehicles have leveraged reinforcement learning to dissipate traffic waves [34, 32, 22]. In fact, many factors can perturb the stability and cause the flow to collectively oscillate. Stability requires the agents to be accurate and reactive. However, driver behaviour, vehicle control, environmental perception, and dynamic aspects are intrinsically subject to fluctuations, inaccuracies, reaction time, and latency.

In this contribution, we first show that white Gaussian noise in a stable nonlinear car-following model - namely the *Adaptive Time Gapf* (ATG) model - can destabilize the system, inducing a phase transition from laminar to periodic dynamics. Analogous to Kapitza’s pendulum, the uniform solution remains stable for small perturbations, while an oscillatory solution with stop-and-go waves becomes stable for perturbations larger than a critical threshold. Stop-and-go waves are classically understood in the literature as a linear instability in a deterministic framework. Here, however, we show that nonlinear instabilities, driven solely by noise, can trigger oscillatory dynamics in an unconditionally linearly stable model when noise amplitude is sufficiently large. This noise-induced collective behaviour can be considered a type of stochastic resonance and stochastic stabilisation. In addition, we show that a simple linear transformation of the model, which amplifies its response and includes a positive acceleration bias, can compensate for the noise effects and significantly improve the stability of the uniform solution. Some simulations replicating Sugiyama’s experiment illustrate the results.

2 Reviewing car-following models and traffic instabilities

The first studies pointing out instability phenomena in vehicle single files date back to the early 1950s, with the pioneering work of Reuschel [49] and, a few years later, Pipes et al. [48]. These groundbreaking studies examined the behaviour of road vehicles using first- and second-order models without delay. By the late 1950s, research expanded to include delays in linear models, as in [30, 19, 5, 28], or in nonlinear models, as in [43, 15]. These prolific years laid the foundations for many fundamental stability concepts using linear algebra [49], Laplace transforms [48, 30, 19], alongside with Fourier analysis [5], see [47] for a survey. Conceptually, researchers differentiate between platoon stability - relevant for finite systems with open boundaries — and string stability, which applies to infinite systems or systems with periodic boundaries. The notions of damped stability, characterised by oscillatory behaviour, and overdamped stability, with lack of oscillations, were also formalised during this period [28]. An important physical insight is the detrimental effect of delay and inertia on flow stability. Unstable models amplify perturbations, leading to the emergence of traffic waves. This represented a significant improvement over earlier fluid-dynamics-based models [37, 50] which are inherently stable and fail to capture such phenomena.

Another fundamental concept was established in the late 1950s. It consists of maintaining a constant time gap with the preceding vehicle. In fact, the existence of a phenomenological relationship between speed and distance can be traced back to one of the earliest traffic measurements in [17]. It was later called the California Code in the literature [5]. Such concept was physically related to safety braking distances in the early 1980s [16]. Nowadays, the existence of an equilibrium relationship between speed and spacing, e.g., a constant time gap strategy with linear speed/spacing relationship, is assumed in most of modern car-following models through optimal velocity (OV) functions [2, 23] or desired time gap [58, 55]. Even norms for adaptive cruise control system recommend to maintain a constant time gap with the predecessor, ranging for instance from 0.8 to 2.2 s in ISO standards [21].

2.1 Optimal velocity models and their stability conditions

Stability analysis experienced a period of decline after its initial prominence, interrupted in the 1970s by the first studies of multi-anticipatory models [4]. It regained momentum in the late 1990s with the advent of nonlinear models, despite earlier recognition that the stability of such models posed significant challenges [15]. In 1995, simulations of the *Optimal Velocity Model* [2] revealed that specific nonlinear optimal velocity functions can exhibit phase transitions in between two stable stationary states under certain parameter settings: a homogeneous state and a heterogeneous state characterised by backward propagating stop-and-go waves.

Optimal velocity models Denoting as $x_n(t)$ the position of the vehicle n at time t , $v_n(t) = dx_n(t)/dt$ its velocity and $\Delta x_n(t) = x_{n+1}(t) - x_n(t)$ the distance to the predecessor, the OV model is given by the differential equation [2]:

$$\frac{dv_n(t)}{dt} = \frac{1}{\tau} [V(\Delta x_n(t)) - v_n(t)], \quad \tau > 0, \quad V \in C^1(\mathbb{R}, \mathbb{R}_+). \quad (1)$$

In the *Full Velocity Difference* (FVD) model, the dynamics is

$$\frac{dv_n(t)}{dt} = \frac{1}{\tau_1} [V(\Delta x_n(t)) - v_n(t)] + \frac{1}{\tau_2} \Delta v_n(t), \quad \tau_1, \tau_2 > 0, \quad V \in C^1(\mathbb{R}, \mathbb{R}_+), \quad (2)$$

where $\Delta v_n(t) = v_{n+1}(t) - v_n(t)$ is the speed difference with the predecessor. In these models, $V \in C^1(\mathbb{R}, \mathbb{R}_+)$ is the optimal velocity function. A typical example of OV function is the hyperbolic tangent

$$V(x) = \frac{V_0}{2} \left[1 + \tanh \left(\frac{x - \ell_0}{T} \right) \right]. \quad (3)$$

Other shapes include the sigmoid function [43]

$$V(x) = V_0 \left[1 - \exp \left(-\frac{x - \ell}{T} \right) \right], \quad (4)$$

which is also used to model pedestrian dynamics [63], or the part-linear form [44]

$$V(x) = \text{smin} \left\{ V_0, \text{smax} \left\{ 0, \frac{x - \ell}{T} \right\} \right\}, \quad (5)$$

where smin and smax are smooth minimum and maximum functions. These OV functions are based on three parameters: $\ell \geq 0$ corresponds to the length of the vehicle, $T > 0$ to the desired time gap, and $V_0 > 0$ to the desired (maximal) speed.

Adaptive time gap model In contrast to classical OV models that relax the speed to a desired (or optimal) speed function that depends on the gap [2, 23], the adaptive time gap (ATG) car-following model [55] is obtained by relaxing the time gap

$$T_n(t) = \frac{g_n(t)}{v_n(t)}, \quad g_n(t) = \Delta x_n(t) - \ell, \quad (6)$$

which is the time taken by a vehicle to reach the vehicle in front, assuming that the speed is constant and the speed of the vehicle in front is zero. Here $\ell > 0$ corresponds to the length of the vehicles. The dynamics for the time gap is given by

$$\frac{dT_n(t)}{dt} = \frac{1}{\tau} (T - T_n(t)), \quad \tau, T > 0,$$

where $\tau > 0$ is a sensitivity parameter and $T > 0$ is the desired time gap. Using the speed and distance variables, the ATG model in its Newtonian form is given by

$$\frac{dv_n(t)}{dt} = \frac{1}{T_n(t)} \left[\frac{1}{\tau} [\Delta x_n(t) - V^{-1}(v_n(t))] + \Delta v_n(t) \right], \quad (7)$$

where $V^{-1}(v) = Tv + \ell$ is the inverse of the optimal velocity function which is assumed to be affine. As we will see in the following, the ATG model is unconditionally linearly stable for any $\tau, T > 0$ and $\ell \geq 0$ [27]. However, the introduction of white noise in the dynamics will induce a phase transition to collective oscillatory behaviour with stop-and-go waves.

Linear stability conditions Consider the general car-following model

$$\frac{dv_n(t)}{dt} = F(\Delta x_n(t), v_n(t), v_{n+1}(t)) \quad (8)$$

where $F \in C^1(\mathbb{R}^3, \mathbb{R})$. Suppose that there exists an equilibrium solution $(v^*, \Delta x^*)$ such that

$$F(\Delta x^*, v^*, v^*) = 0. \quad (9)$$

Linearising the speed dynamics around the uniform equilibrium solution gives

$$\frac{d\tilde{v}_n(t)}{dt} = a\Delta\tilde{x}_n(t) + b\tilde{v}_n(t) + c\tilde{v}_{n+1}(t) \quad (10)$$

where

$$\Delta\tilde{x}_n(t) = \Delta x_n(t) - \Delta x^*, \quad \tilde{v}_n(t) = v_n(t) - v^*, \quad (11)$$

while, with $F : (x, y, z) \mapsto F(x, y, z)$,

$$a = \frac{\partial F}{\partial x}(\Delta x^*, v^*, v^*), \quad b = \frac{\partial F}{\partial y}(\Delta x^*, v^*, v^*), \quad c = \frac{\partial F}{\partial z}(\Delta x^*, v^*, v^*). \quad (12)$$

It is easy to check that the characteristic equation of the linear dynamics (10) reads

$$\zeta^2 + \zeta(b + c \exp(i\theta)) + a(1 - \exp(i\theta)) = 0, \quad \zeta \in \mathbb{C}, \quad \theta \in (0, 2\pi). \quad (13)$$

The characteristic equation is a second-order polynomial with complex coefficients. The system is linearly stable if the real part of the roots ζ_θ are nonpositive for all $\theta \in (0, 2\pi)$. This holds true if [56], [59, Chap. 15]

$$a > 0, \quad b < 0, \quad \text{and} \quad b^2 - c^2 \geq 2a. \quad (14)$$

These conditions can be recovered by using general stability conditions for complex polynomials in [11, Th. 3.2] which are generalisation of the Hurwitz conditions. In addition, the system with $c > 0$ is overdamped stable, i.e., it does not present oscillation during the stabilisation phase, if [26]

$$a > 0, \quad b < 0, \quad \text{and} \quad \frac{a}{c} + b + c \leq 0. \quad (15)$$

Note that the overdamped stability condition is stronger than the simple stability, i.e., $(15) \Rightarrow (14)$. The conditions are sufficient for any finite system and become exact for infinite systems.

For example, for the FVD model (2) where $V'(\Delta x^*) = 1/T$, the partial derivatives at equilibrium are given by

$$a_{\text{FVD}} = \frac{1}{T\tau_1}, \quad b_{\text{FVD}} = -\frac{1}{\tau_1} - \frac{1}{\tau_2}, \quad c_{\text{FVD}} = \frac{1}{\tau_2}. \quad (16)$$

The linear stability condition (14) is

$$\tau_1, \tau_2 > 0, \quad 0 < 2\tau_1\tau_2 / (2\tau_1 + \tau_2) \leq T, \quad (17)$$

while the overdamped stability condition (15) is given by

$$\tau_1 > 0, \quad 0 < \tau_2 \leq T. \quad (18)$$

For the ATG model (7), the partial derivatives at equilibrium are

$$a_{\text{ATG}} = \frac{1}{T\tau}, \quad b_{\text{ATG}} = -\frac{1}{\tau} - \frac{1}{T}, \quad c_{\text{ATG}} = \frac{1}{T}, \quad (19)$$

and the stability conditions (14) and (15) hold true for any $\tau, T > 0$. The model is unconditionally linearly overdamped stable, hence its prevalence for automated driving systems [27].

Linear stability analysis underscores the central role of inertia and nonlinear mechanisms in explaining stop-and-go traffic dynamics. Hopf bifurcation allows to characterise the phase transition from uniform (laminar) dynamics to oscillatory behaviour with stop-and-go waves [46, 47, 56]. Different perturbation dynamics can be identified, including convective upstream, stationary, and convective downstream modes [64]. Subsequent research with reductive perturbation methods derives macroscopic wave patterns given by the Korteweg-de Vries (KdV) equation [29] and the modified KdV equation [42] from optimal velocity models. Additionally, nonlinear models can demonstrate metastable behaviour, exhibiting multiple stationary dynamics depending on initial conditions [54]. These results paved the way for the analysis of stop-and-go wave phenomena and phase transitions in traffic flow based on a linear instability of inertial, i.e., second-order, nonlinear models [14, 47].

2.2 Stochastic models

The inertia-induced linear instability of classical car-following models explains well the phenomena of spontaneous perturbation amplification recently observed in experiments with ACC-equipped vehicles [18, 38]. Indeed, the response times of the ACC-systems seem too large to fulfil basic linear stability conditions [39]. Another alternative modelling approach of traffic instabilities relies on stochastic aspects. Pioneering work in this area have been done using discrete cellular automata and interacting particle systems [3, 25, 24, 20], [51, Chap. 8.1]. More recently, continuous modelling approaches based on stochastic differential equation systems incorporate additive noise [57, 61, 33]. A general stochastic car-following model is given by

$$\begin{cases} dx_n(t) = v_n(t) dt \\ dv_n(t) = F(\Delta x_n(t), v_n(t), \Delta v_{n+1}(t)) dt + \sigma dW_n(t), \end{cases} \quad (20)$$

where $F \in C^1(\mathbb{R}^3, \mathbb{R})$ is a continuous and derivable nonlinear function governing the motion, while σdW_n is a white noise with W_n a standard Wiener process and $\sigma \geq 0$ the noise amplitude.

Linear or near-linear stochastic models Linear or near-linear stochastic models derived from optimal velocity car-following models are given by [57, 61, 33, 62, 12]:

$$dv_n(t) = -\kappa[V(\Delta x_n(t)) - v_n(t)]dt + c\Delta v_n(t)dt + \sigma dW_n(t), \quad \kappa < 0, \quad c \geq 0, \quad (21)$$

where V is the optimal velocity function. We recover a stochastic version of the OV model for $c = 0$, whereas a stochastic FVD model is recovered for $c > 0$. Systems with linear OV functions V are ergodic multidimensional Ornstein-Uhlenbeck processes having a stable dynamics with a single invariant Gaussian distribution [62, 12]. More realistic models have nonlinear OV functions V (see, e.g., [57]). Another example of near-linear stochastic model is the inertial car-following model [54]

$$dv_n(t) = K \left(1 - \frac{2v_n(t)T + \ell}{\Delta x_n(t) - \ell} \right) dt + \frac{Z^2(\Delta v_n(t))}{2\Delta x_n(t)} dt - 2Z(v_n(t) - V_0)dt + \sigma dW_n(t), \quad K > 0, \quad (22)$$

where $Z(x) = (x + |x|)/2$ is the positive part of x and $T > 0$ the desired time gap. These models include nonlinear components through the OV function or sensitivity coefficients. However, they behave mainly as linear models when stable and do not describe a phase transition as the noise volatility increases, except in subcritical regimes [60]. In fact, the stability condition is not affected by white noise with linear models.

Nonlinear stochastic models The *intelligent driver* (ID) model is a well-known nonlinear car-following model introduced in the early 2000's [58]. The stochastic extension of this model (SID) studied more recently [60] is given by

$$dv_n(t) = \alpha \left(1 - \left(\frac{f(v_n(t), v_{n+1}(t))}{\Delta x_n(t) - \ell} \right)^2 - \left(\frac{v_n(t)}{V_0} \right)^4 \right) dt + \sigma dW_n(t), \quad (23)$$

where

$$f(v_n, v_{n+1}) = s_0 + T v_n - v_n \frac{v_{n+1} - v_n}{2\sqrt{\alpha\beta}}, \quad s_0, \alpha, \beta > 0. \quad (24)$$

In contrast to the previous linear and near-linear models, the SID model is strongly nonlinear. It describes a phase transition resulting from a subcritical instability as the noise volatility increases [60]. This transition is caused by both the nonlinearity and the underlying linear instability of the deterministic intelligent driver model. It only occurs in the vicinity of the critical parameter setting. Note that state-dependent noise models based on the Cox-Ingersoll-Ross process also exhibit phase transition as the noise volatility increases, see, for example, [45, 66]. In these models, the transition also occurs from a linear instability because the noise function depends on the system state, rather than the form of the OV function as it does in deterministic car-following models.

3 Noise-induced phase transition

In this section, we point out through simulations using the ATG model that introducing white Gaussian noise into gap measurements leads to nonlinear instability of the uniform solution and the emergence of stop-and-go oscillatory dynamics. We interpret this noise-induced collective behaviour using the analogy of the Kapitza inverted pendulum and the concepts of stochastic resonance and stochastic stabilisation.

3.1 Stochastic ATG model

In [8], a noise term is added to the acceleration function of the ATG model. In this article, we introduce noise into the measurement of the gap. Human perception of distances is indeed imperfect. Distance sensors also have a limited accuracy, particularly in challenging conditions, e.g., due to bad weather or road curvature. We expect the noise to be correlated over time, using, e.g., an Ornstein-Uhlenbeck process, and dependent on the measured distance; estimation is typically more accurate for small distances. However, to keep the modelling approach minimalistic, we use a simple white noise, independent of the system state and uncorrelated in time. Additionally, rather than estimating the noise amplitude empirically, we carry out simulations by varying the noise amplitude range.

Time-continuous stochastic model The stochastic ATG model including white noise in the gap is given by

$$dv_n(t) = \frac{\frac{1}{\tau} [g_n(t) + \sigma \xi_n(t) - T v_n(t)] + \Delta v_n(t)}{T_\varepsilon(g_n(t) + \sigma \xi_n(t), v_n(t))} dt, \quad (25)$$

where ξ_n denotes independent standard Gaussian noise uncorrelated in time, i.e., $\langle \xi_n(t) \xi_n(t') \rangle = \delta(t - t')$, and $\sigma > 0$ is the noise amplitude. Here, the time gap is approximated using the smooth minimum (resp. maximum) T_ε bounded between T_{\min} and T_{\max} , $0 < T_{\min} < T_{\max}$,

$$T_\varepsilon(g, v) = f_\varepsilon \left(T_{\min}, f_{-\varepsilon} \left(T_{\max}, \frac{g}{f_\varepsilon(0, v)} \right) \right), \quad (26)$$

where f_ε is the *LogSumExp* function given by

$$f_\varepsilon(x, y) = \varepsilon \log (\exp(x/\varepsilon) + \exp(y/\varepsilon)), \quad \varepsilon > 0. \quad (27)$$

The function $f_\varepsilon(x, y)$ converges to the maximum of x and y as $\varepsilon \rightarrow 0^+$ and to the minimum as $\varepsilon \rightarrow 0^-$. In the following, we use $\varepsilon = 0.01$. This smoothing of the dynamics avoids singularities when the vehicles collide due to noise or when the speed is zero.

Time-discrete stochastic model The numerical simulations of the stochastic ATG model are performed using an implicit Euler scheme for the vehicle positions while the speeds are determined using an explicit scheme. This coupled numerical scheme is given by

$$\begin{cases} x_n(t + \delta t) = x_n(t) + \delta t v_n(t + \delta t) \\ v_n(t + \delta t) = v_n(t) + \delta t \frac{\frac{1}{\tau} [g_n(t) + \sigma \xi_n(t) - T v_n(t)] + \Delta v_n(t)}{T_\varepsilon(g_n(t) + \sigma \xi_n(t), v_n(t))}. \end{cases} \quad (28)$$

The time step of the simulations is defined as $\delta t = 0.01$ s. In addition, the parameter values are the following: $\tau = 5$ s, $T = 0.9$ s, $\ell = 3$ m, $T_{\min} = 0.1$ s and $T_{\max} = 2.5$ s. Here, $\tau = 5$ s is chosen based on statistical estimations [55]. The parameters $\ell = 3$ m and $T = 0.9$ s are calibrated to obtain a mean speed approximately equal to 30 km/h, as requested during the experiment, and a propagation speed of the stop-and-go wave backward of approximately 20 km/h, as empirically observed. In addition, the setting $T_{\max} = 2.5$ s corresponding to the time gap on wave output is used to match the duration of the stop phase. The parameter T_{\min} does not seem to influence the dynamics as long as it remains small, although it is greater than δt .

3.2 Simulation results

In the following, we simulate $N = 22$ vehicles on a single-lane circuit of length $L = 231$ m with periodic boundaries using the stochastic ATG model (25) to mimic the conditions of the experiment by Sugiyama et al. [53] (see Fig. 2). An online simulation module is available at: https://www.vzu.uni-wuppertal.de/fileadmin/site/vzu/Noise-Induced_Stop-and-Go_Modelling_and_Control.html?speed=0.7.

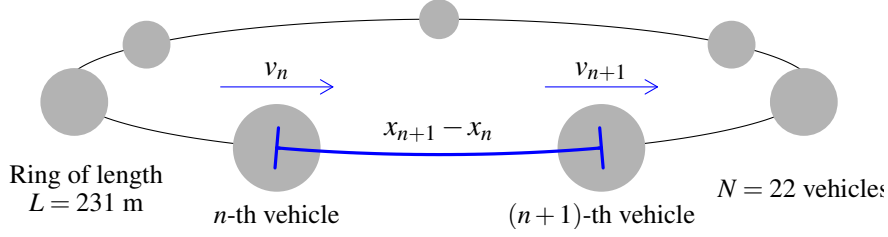


Figure 2: Replica of the experiment by Sugiyama et al. [53].

Trajectories from a single simulation Fig. 3 shows an example of simulated trajectories using the stochastic ATG model (28) over 250 seconds. The initial vehicle positions and speeds are the same as in the experiment by Sugiyama et al. [53]. The noise amplitude is $\sigma = 2.8$ m. A single stop-and-go wave emerges after approximately two minutes, as observed in the experiment, compare Figs. 1 and 3. The wave formation time, its amplitude, and propagation speed are all relatively well described. Additionally, the sequences of mean speed and gap standard deviation exhibit similar trends to those observed in the experiment. However, the trajectories and mean sequences differ qualitatively from those observed in the experiment. They appear much more regular, primarily because all vehicles behave identically in the model. In fact, there is no heterogeneity in driving style that we would expect from real drivers. Furthermore, the noise affects only the distance variable, which is an input smoothed by the model. Adding noise directly to the acceleration makes the trajectories less regular, see [8, Fig. 4].

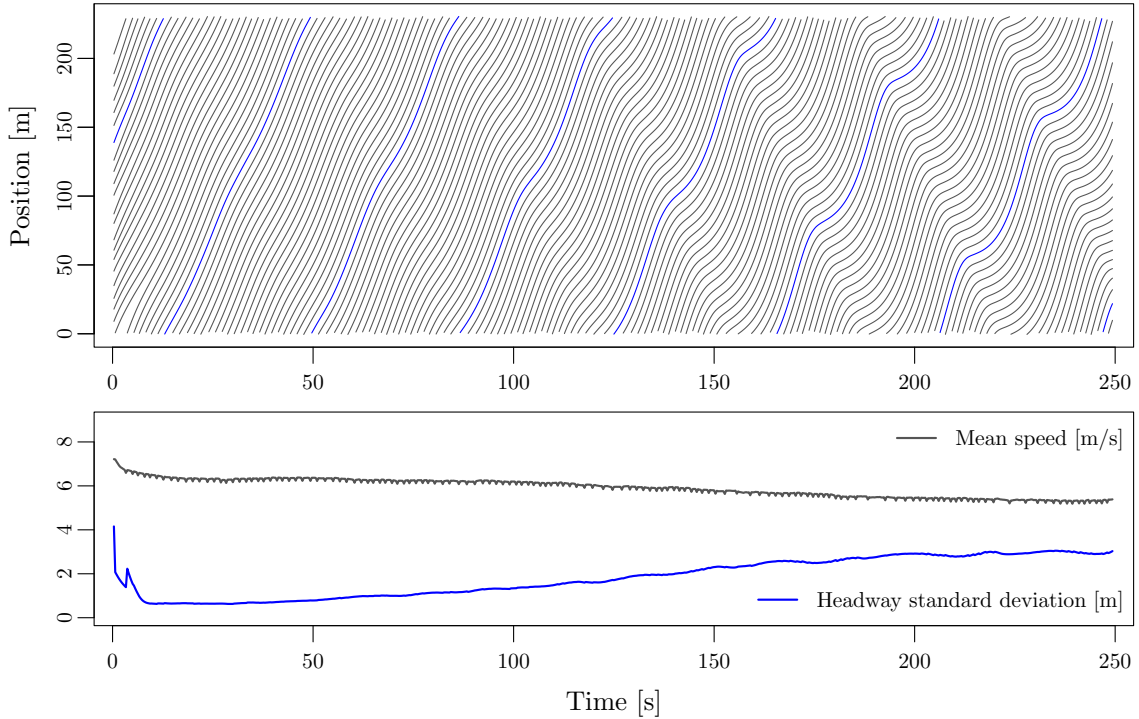


Figure 3: Simulated trajectories of 22 vehicles on a 231-metre circuit as in the experiment by Sugiyama et al. [53] using the stochastic ATG model (28) where $\sigma = 2.8$ m. The trajectories can be simulated on-line at: https://www.vzu.uni-wuppertal.de/fileadmin/site/vzu/Noise-Induced_Stop-and-Go_Modeling_and_Control.html?speed=0.7.

Noise-induced transition to stop-and-go dynamics Several independent simulations are performed by varying the noise amplitude σ from 1 to 6 m in steps of 0.1 m. All the other parameters $\tau = 5$ s, $T = 0.9$ s, $\ell = 3$ m, $T_{\min} = 0.1$ s, and $T_{\max} = 2.5$ s remain constant. We repeat the simulations $K = 100$ times for each value of the noise amplitude, starting from uniform initial conditions. The simulations are run for $t_S = 1000$ seconds to reach a stationary state, before we average over time the spacing standard deviation

$$\Phi(t_S, t_M) = \frac{\delta t}{t_M} \sum_{t=t_S}^{t_S+t_M} \sqrt{\frac{1}{N-1} \sum_{n=1}^N (\Delta x_n(t) - L/N)^2} \quad (29)$$

during the next $t_M = 100$ seconds. The results are shown in Fig. 4. A phase transition is clearly observed when the noise amplitude exceeds approximately $\sigma \approx 2.6$ m. Additionally, the mean speed drops by around 15% as the stop-and-go dynamics emerge (see the subplot in Fig. 4). A similar capacity reduction is also evident in the experiment, see Fig. 1 and [52, Fig. 6.6]. This decrease of the mean speed is due to the nonlinear form of the ATG model and its asymmetric behaviour during braking and acceleration stop-and-go phases. Interestingly, an optimal noise amplitude for the emergence of waves can be identified as around $\sigma \approx 2.7$ m. Beyond this optimal noise amplitude, the spacing standard deviation decreases progressively until it reaches a low constant for values of σ beyond 4.5 meters, meaning that no stop-and-go waves arise.

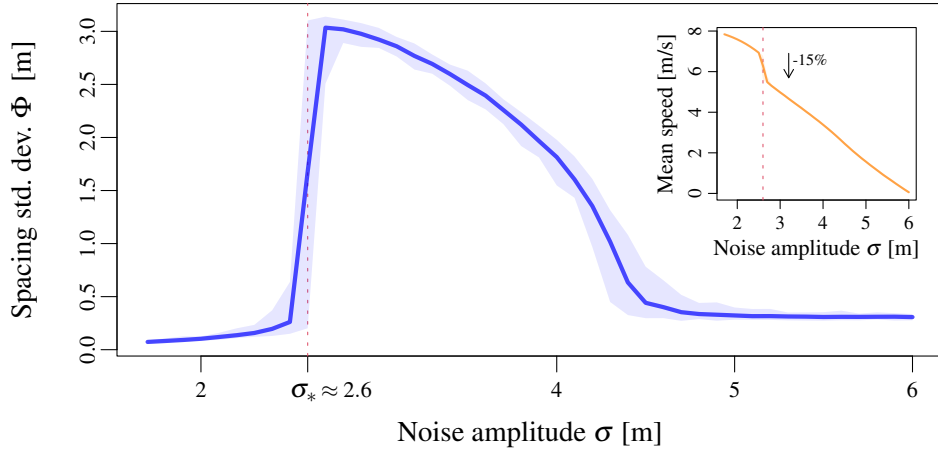


Figure 4: Gap standard deviation for the 22 vehicles on the 231 m circuit (replica of the Sugiyama experiment) with the noisy ATG model (25) obtained from variation of the noise amplitude. The continuous lines are the averaged gap standard deviations of $K = 100$ simulations, while the coloured areas are the min/max ranges. A phase transition arises from stable uniform solutions to stop-and-go dynamics as the noise amplitude increases. In addition, an optimal noise amplitude for the emergence of waves can be identified.

Influence of the model's parameters on stability The critical noise amplitude threshold for wave formation depends on the density level and the values of the model parameters. Increasing the values of the parameters ℓ and T , i.e. reducing the mean vehicle speed, results in stop-and-go dynamics emerging at a lower noise amplitude. More precisely, a linear relationship can be identified between the parameter ℓ controlling the mean gap and the critical noise amplitude, see Fig. 5, left panel. In fact, the waves emerge

when the noise amplitude is higher than around 35% of the mean gap. A nonlinear exponentially decreasing relationship occurs with the time gap parameter T , see Fig. 5, middle panel. Surprisingly, reducing the time gap, i.e., increasing the mean vehicle speed, improves stability. The relationship with the relaxation time parameter τ is more complex. It is nonmonotonic, see Fig. 5, right panel. The stability of the model is most critical at approximately $\tau = 3$. Beyond this point, more reactive or smoother behaviour improves stability.

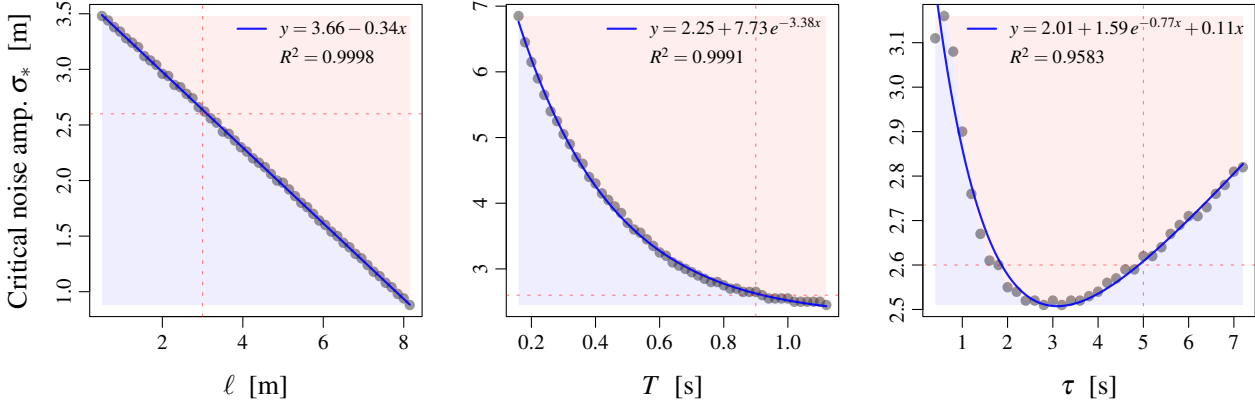


Figure 5: Critical noise amplitude threshold according to the three main parameters of the ATG model (from left to right): ℓ , T , and τ . The system is unstable and waves propagate above the critical curve (red part) while the system is stable below it (blue part).

Noise driven by the Ornstein-Uhlenbeck process For modelling purposes and sake of simplicity, it is convenient to assume that white noise affects the measurement of the gap. However, humans and vehicles are not atomistic. In fact, it would be more realistic to assume that measurement perturbations are correlated over time. In this context, we carried out further simulations using independent Ornstein-Uhlenbeck processes, denoted by $\tilde{\xi}_n$, instead of the white noise $\sigma\xi_n(t)$ in (25).

The ATG model driven by the Ornstein-Uhlenbeck process is given by

$$\begin{cases} dv_n(t) = \frac{\frac{1}{\tau} [g_n(t) + \tilde{\xi}_n(t) - Tv_n(t)] + \Delta v_n(t)}{T_\epsilon(g_n(t) + \tilde{\xi}_n(t), v_n(t))} dt, \\ d\tilde{\xi}_n(t) = -\frac{1}{\beta} \tilde{\xi}_n(t) dt + \tilde{\sigma} dW_n(t), \end{cases} \quad (30)$$

where W_n are standard Wiener processes. The Ornstein-Uhlenbeck process $\tilde{\xi}_n$ is a Gaussian process with asymptotic expected value zero and variance $0.5\beta\tilde{\sigma}^2$. Unlike the white noise model, which is uncorrelated over time, the time correlation of the Ornstein-Uhlenbeck process is given by:

$$\langle \tilde{\xi}_n(t), \tilde{\xi}_n(t') \rangle = \frac{1}{2} \beta \tilde{\sigma}^2 e^{-|t-t'|/\beta}.$$

We set the relaxation time $\beta = 5$ s to introduce a large time correlation of the noise.

A similar phase transition can be observed from about $\tilde{\sigma} > 6.5$ m/s^{1/2}, see Fig. 6 and compare with Fig. 4. In fact, further simulation results show that comparable noise-induced oscillations occur when the

noise is added to the acceleration, to the speed difference, or to a combination of the acceleration, the speed difference, and the gap. In [8], white and state-dependent noises that vanish when the speed approaches zero are introduced into the acceleration function of the ATG model, yielding similar qualitative phase transitions. The nature of the noise does not appear to be the primary factor in the phase transition. The most important aspect is that the system is perturbed stochastically.

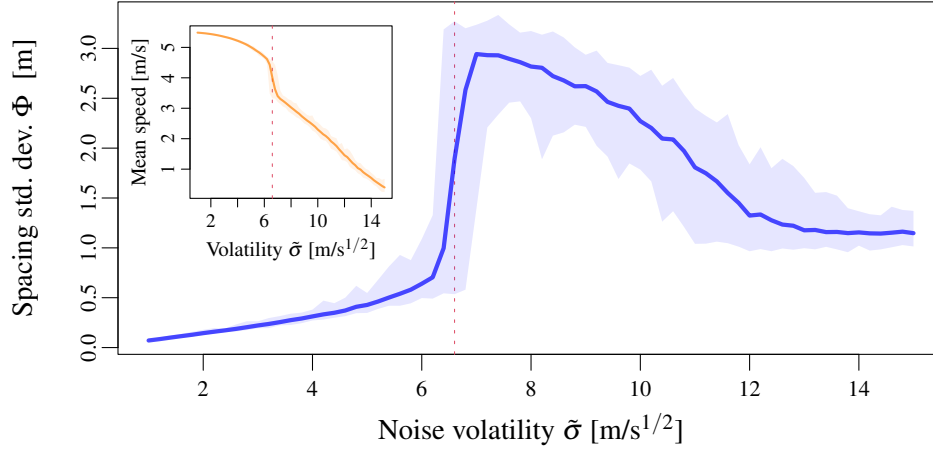


Figure 6: Gap standard deviation for the 22 vehicles on the 231 m circuit (replica of the Sugiyama experiment) with the noisy ATG model (30) driven by the Ornstein-Uhlenbeck process. The noise volatility $\tilde{\sigma}$ vary from 0 to 15 $\text{m/s}^{1/2}$. Here, $\beta = 5$ s to introduce a large time-correlation of the noise. The continuous lines are the averaged gap standard deviations of $K = 100$ simulations, while the coloured areas are the min/max ranges. As with the white noise model, a phase transition arises from stable uniform solutions to stop-and-go dynamics as the noise increases, compare with Figure 4.

Analogy with physical systems The simulation results demonstrate that oscillatory stop-and-go waves caused by noise occur with many different types of noise. These include white noise and time-correlated noise, as well as noise acting on the gap, speed difference or acceleration. The uniform solution is stable for small perturbations but becomes unstable for large ones, resulting in stop-and-go dynamics. However, the ATG model is unconditionally linearly stable. The uniform solution is stable for all initial conditions, whether they are jam wave or simply random configurations. Therefore, stop-and-go dynamics result from nonlinear instability purely induced by noise. This phenomenon is analogous to Kapitza’s pendulum, where the stable solution switches to an inverted pendulum when perturbed. It can also be interpreted as a stochastic resonance phenomenon. In fact, the noise causes the system to oscillate at the largest wavelength. Although this hidden frequency is unstable, it represents the most stable oscillatory configuration of the system. For the ATG model, the root of the characteristic equation (13) with the largest real part is that for $\theta \rightarrow 0$.

The noise causes the system to switch from the laminar state to the oscillatory state. In addition, an optimal noise amplitude can be identified for the emergence of waves. These are characteristic features of stochastic resonance in bistable systems [13]. In this study, however, the noise directly affects the stationary states of the system and their stability. The uniform equilibrium is stable in the deterministic case. The system converges to a laminar streaming regardless of the initial conditions. The oscillatory configuration is unstable without perturbations, even locally. Under large perturbations, the uniform equilibrium

is unstable and the oscillatory solution with stop-and-go waves becomes stable instead. Nevertheless, if the perturbed system reaches an oscillatory configuration with stop-and-go waves the flow will become laminar again if the noise disappears. This behaviour differs from that of classical stochastic resonance, where noise merely facilitates transitions between two locally stable equilibrium states. Here, the transition to oscillatory dynamics is purely induced by noise. It could be interpreted as a form of stochastic stabilization [1] since the noise enables oscillatory solutions with stop-and-go waves to become stable. However, unlike in classical stochastic stabilisation phenomena, the stabilised solution is not a stationary equilibrium but rather an oscillatory collective pattern in response to perturbations.

3.3 Stabilisation of the dynamics

In real-world scenarios, uncertainties regarding the gap and velocity of the leading vehicle present significant challenges for ACC systems. The ACC controller must ensure that these uncertainties do not result in excessive acceleration and braking events, which could lead to an uncomfortable or even unsafe driving experience [40]. To address this, ACC systems are designed to be less reactive, incorporating filtering and smoothing mechanisms. The treatment of the resulting dilemma between comfortable driving experience and traffic stability is still an open research question [65].

To address the issue of instability within the stochastic Adaptive Time Gap (ATG) model, we propose an affine transformation of the system dynamics. This approach aims to suppress noise-induced nonlinear instabilities of the uniform solution. The transformed model is defined by

$$dv_n(t) = \left[A \frac{\frac{1}{\tau} (g_n(t) + \sigma \xi_n(t) - T v_n(t)) + \Delta v_n(t)}{T_\varepsilon(g_n(t) + \sigma \xi_n(t), v_n(t))} + B \right] dt, \quad A > 0, B \in \mathbb{R}, \quad (31)$$

where A represents a scale factor and B denotes an acceleration bias. Specifically, $A > 1$ amplifies the control response to quickly counteract noise effects while $B > 0$ introduces a bias towards acceleration to prevent excessive deceleration and avoid wave amplification. The simulations demonstrate that for sufficiently large values of A and B the system can effectively dissipate waves even under high noise amplitudes. As shown in Fig. 7, when $A \geq 1.2$ and $B \geq 0.2 \text{ m/s}^2$, the spacing standard deviation approaches zero even for high values of the noise amplitudes σ , indicating successful wave dissipation.

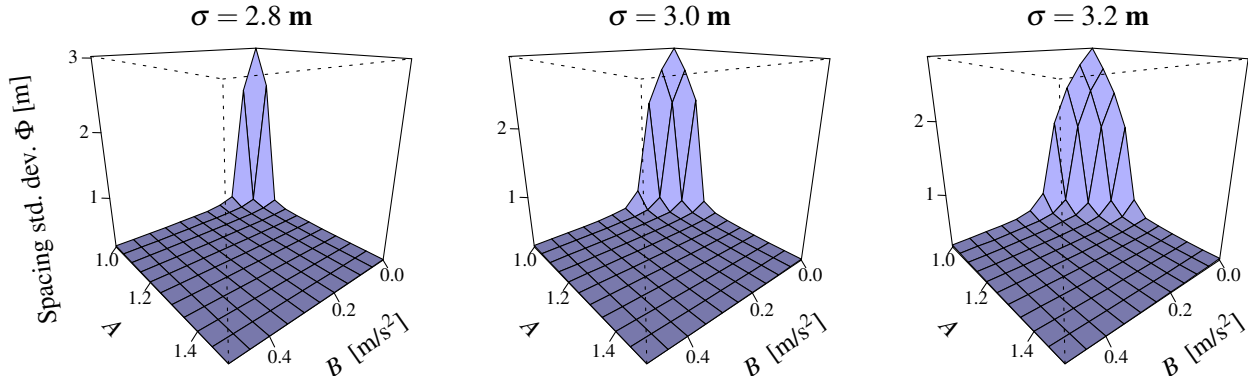
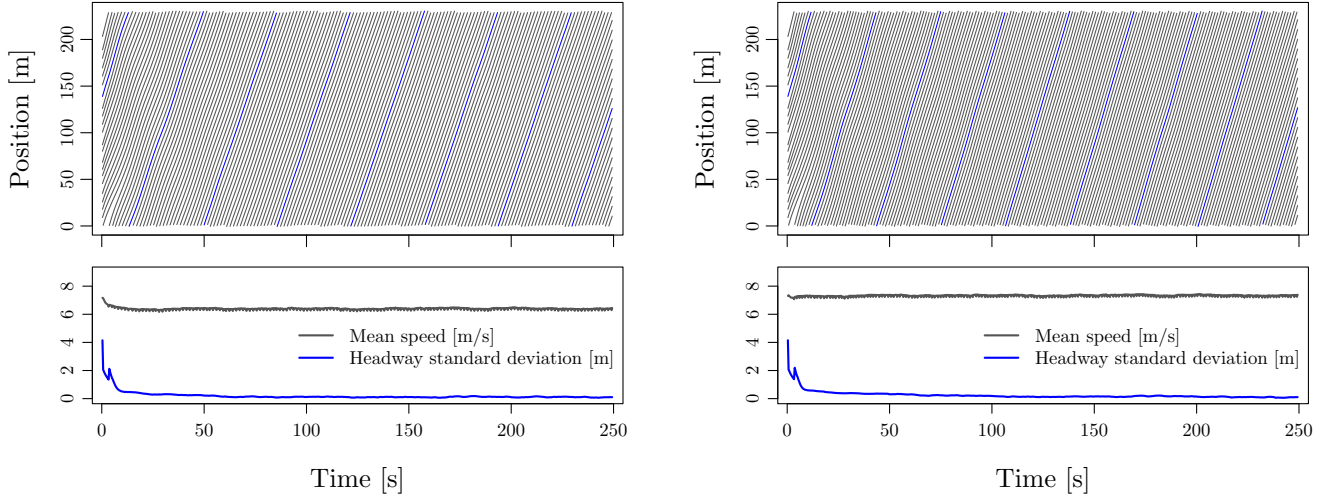


Figure 7: Average spacing standard deviation for 22 vehicles on a 231 m circuit (replicating the Sugiyama experiment) using the stochastic ATG model (31), with varying scale factor A and acceleration bias B . The spacing deviation approaches zero, indicating wave dissipation, as A and B increase.

The beneficial effects of this transformation are further illustrated in Fig. 8 where we replicate the experiment from Fig. 3. Keeping all conditions identical, we introduce the tuning parameters $A = 1.2$, $B = 0 \text{ m/s}^2$ in Fig. 8 (a) and the combination $A = 1$, $B = 0.2 \text{ m/s}^2$ in Fig. 8 (b). In both cases, stop-and-go waves are entirely eliminated. In addition, the speed is slightly increased when the bias B is strictly positive, see Fig. 8 (b), grey curve in the lower panel. Indeed, when positive, the acceleration bias parameter B increases the system's equilibrium speed.



(a) Trajectories with $\sigma = 2.8 \text{ m}$, $A = 1.2$, $B = 0 \text{ m/s}^2$.

(b) Trajectories with $\sigma = 2.8 \text{ m}$, $A = 1$, $B = 0.2 \text{ m/s}^2$.

Figure 8: Simulated trajectories of 22 vehicles on a 231-metre circuit using the stochastic ATG model (31), compared to the baseline in Fig. 3.

While the affine modification (31) improves stability, it is not without trade-offs. High values of the factor A can result in uncomfortable levels of acceleration and a positive bias B may compromise safety by reducing the time gap to the lead vehicle. In fact, the resulting equilibrium time gap becomes:

$$T^*(v) = \frac{T}{1 + \frac{B\tau}{Av}}. \quad (32)$$

When $B \geq 0$, this effective time gap $T^*(v)$ decreases as speed v approaches zero and asymptotically approaches the nominal gap T at higher speeds. It is a strictly increasing function of v but always smaller than T . From a safety standpoint, this can be problematic at low speeds due to reduced headway. However, from a performance perspective, especially in vehicle platooning, this behaviour is advantageous. Reduced time gaps typically enhance throughput and efficiency. Interestingly, in contrast to traditional approaches, where stability improves at the cost of increased time gaps, this method offers an alternative solution. By allowing $T^*(v)$ to increase with speed, the system maintains safety at higher velocities by improving stability and mitigating noise-induced instabilities that typically destabilize traffic flow.

4 Discussion and Conclusion

Gaussian noise in the nonlinear ATG car-following model can lead to the emergence of oscillatory dynamics and stop-and-go waves, although the model is unconditionally linearly stable and the noise is white. In fact, the uniform solution remains stable for small perturbations, but becomes unstable and gives way to stop-and-go dynamics for large perturbations. This applies to many different types of noise, including white noise and time-correlated noise, as well as noise acting on the gap, speed difference, or acceleration. Similar to Kapitza's pendulum in a stochastic framework, the noise in the nonlinear dynamics affects the stability of the system and induces a phase transition including a metastable regime. Here, the waves result from a nonlinear instability in contrast to classical delayed and inertial car-following models where the transition is based on a linear instability. Intriguingly, a simple affine transformation of the model allows the waves to dissipate and the stability of uniform solutions to be recovered. Similar results have been observed using heterogeneous car-following models [9]. Amplifying the response and adding a positive bias seems to be an effective strategy to mitigate the instabilities induced by the noise and other heterogeneity factors.

Beyond improving stability, the affine transformation of the model has notable implications. Large factors A can cause excessive acceleration, while positive biases B may compromise safety by reducing the effective time gap, especially at low speeds. This equilibrium time gap increases with speed but remains below the desired time gap T , thus potentially posing safety concerns. However, this behaviour enhances performance—particularly in platooning—since stability improves with reduced time gaps. Unlike traditional approaches where increasing the time gap boosts stability at the cost of efficiency, this method leverages a speed-dependent time gap to mitigate noise-induced nonlinear instability while maintaining high performance. It would be interesting to investigate whether the affine transformation of the model could also compensate for the linear instabilities of delayed or inertial models. Preliminary simulation results show that this is not the case for the delayed or lag ATG model. This is not surprising. Although the stop-and-go waves in the case of a linear instability due to delay and inertia or a nonlinear instability due to noise are qualitatively similar, the mechanisms involved are different. Specific compensators are therefore required to reduce delays in the dynamics. Unified algorithms need to be developed that are robust to both stochastic perturbations and delays in the dynamics of the system.

Acknowledgement

RK and AT acknowledge the German Research Foundation (Deutsche Forschungsgemeinschaft - DFG) for funding this research, grant number 546728715.

References

- [1] J. A. Appleby and X. Mao. Stochastic stabilisation of functional differential equations. *Systems & Control Letters*, 54(11):1069–1081, 2005.
- [2] M. Bando, K. Hasebe, A. Nakayama, A. Shibata, and Y. Sugiyama. Dynamical model of traffic congestion and numerical simulation. *Physical Review E*, 51(2):1035–1042, 1995.

- [3] R. Barlovic, L. Santen, A. Schadschneider, and M. Schreckenberg. Metastable states in cellular automata for traffic flow. *The European Physical Journal B*, 5:793–800, 1998.
- [4] S. Bexelius. An extended model for car-following. *Transp. Res.*, 2(1):13–21, 1968.
- [5] R. E. Chandler, R. Herman, and E. W. Montroll. Traffic dynamics: studies in car following. *Operations Research*, 6(2):165–184, 1958.
- [6] B. Ciuffo, K. Mattas, M. Makridis, G. Albano, A. Anesiadou, Y. He, S. Josvai, D. Komnos, M. Pataki, S. Vass, et al. Requiem on the positive effects of commercial adaptive cruise control on motorway traffic and recommendations for future automated driving systems. *Transportation research part C: emerging technologies*, 130:103305, 2021.
- [7] L. Duckstein. Control of traffic in tunnels to maximize flow. *Highway Research Record*, 154, 1967.
- [8] O. Dufour, J. Cordes, A. Nicolas, A. Tordeux, D. Rodney, and A. Schadschneider. Noise-induced transition to stop-and-go waves in single-file traffic rationalized by an analogy with kapitza’s inverted pendulum, 2025.
- [9] M. Ehrhardt and A. Tordeux. Stability of heterogeneous linear and nonlinear car-following models. *Franklin Open*, page 100181, 2024.
- [10] M. R. Flynn, A. R. Kasimov, J.-C. Nave, R. R. Rosales, and B. Seibold. Self-sustained nonlinear waves in traffic flow. *Physical Review E—Statistical, Nonlinear, and Soft Matter Physics*, 79(5):056113, 2009.
- [11] E. Frank. On the zeros of polynomials with complex coefficients. *Bulletin of the American Mathematical Society*, 52(2):144–157, 1946.
- [12] M. Friesen, H. Gottschalk, B. Rüdiger, and A. Tordeux. Spontaneous wave formation in stochastic self-driven particle systems. *SIAM Journal on Applied Mathematics*, 81(3):853–870, 2021.
- [13] L. Gammaitoni, P. Hänggi, P. Jung, and F. Marchesoni. Stochastic resonance. *Reviews of modern physics*, 70(1):223, 1998.
- [14] I. Gasser, G. Sirito, and B. Werner. Bifurcation analysis of a class of ‘car following’ traffic models. *Physica D: Nonlinear Phenomena*, 197(3-4):222–241, 2004.
- [15] D. C. Gazis, R. Herman, and R. W. Rothery. Nonlinear follow-the-leader models of traffic flow. *Operations Research*, 9(4):545–567, 1961.
- [16] P. Gipps. A behavioural car-following model for computer simulation. *Transportation Research Part B: Methodological*, 15:105–111, 1981.
- [17] B. Greenshields, J. Thompson, H. Dickinson, and R. Swinton. The photographic method of studying traffic behavior. In *Highw. Res. Board. Proc.*, volume 13, pages 382—389, 1934.
- [18] G. Gunter, D. Gloudemans, R. E. Stern, S. McQuade, R. Bhadani, M. Bunting, M. L. Delle Monache, R. Lysecky, B. Seibold, J. Sprinkle, et al. Are commercially implemented adaptive cruise control systems string stable? *IEEE Transactions on Intelligent Transportation Systems*, 22(11):6992–7003, 2020.

- [19] R. Herman, E. W. Montroll, R. B. Potts, and R. W. Rothery. Traffic dynamics: Analysis of stability in car following. *Operations Research*, 7(1):86–106, 1959.
- [20] Y.-X. Huang, N. Guo, R. Jiang, and M.-B. Hu. Instability in car-following behavior: new nagel-schreckenberg type cellular automata model. *Journal of Statistical Mechanics: Theory and Experiment*, 2018(8):083401, 2018.
- [21] ISO:15622. Intelligent transport systems — adaptive cruise control systems — performance requirements and test procedures, 2018.
- [22] K. Jang, N. Lichtlé, E. Vinitsky, A. Shah, M. Bunting, M. Nice, B. Piccoli, B. Seibold, D. B. Work, M. L. D. Monache, et al. Reinforcement learning based oscillation dampening: Scaling up single-agent rl algorithms to a 100 av highway field operational test. *arXiv preprint arXiv:2402.17050*, 2024.
- [23] R. Jiang, Q. Wu, and Z. Zhu. Full velocity difference model for a car-following theory. *Physical Review E*, 64:017101, 2001.
- [24] J. Kaupuzs, R. Mahnke, and R. Harris. Zero-range model of traffic flow. *Physical Review E*, 72(5):056125, 2005.
- [25] L. Ke-Ping and G. Zi-You. Noise-induced phase transition in traffic flow*. *Communications in Theoretical Physics*, 42(3):369, sep 2004.
- [26] P. Khound, P. Will, and F. Gronwald. Local and string stability conditions of a generalized adaptive cruise control system. In *AmE 2020-Automotive meets Electronics; 11th GMM-Symposium*, pages 29–36. VDE, 2020.
- [27] P. Khound, P. Will, A. Tordeux, and F. Gronwald. Extending the adaptive time gap car-following model to enhance local and string stability for adaptive cruise control systems. *Journal of Intelligent Transportation Systems*, 27(1):36–56, 2023.
- [28] T. Kishi. Traffic dynamics: Analysis as sampled-data control systems. *Journal of the Operations Research Society of Japan*, 2:114–123, 1960.
- [29] T. S. Komatsu and S.-i. Sasa. Kink soliton characterizing traffic congestion. *Physical Review E*, 52(5):5574, 1995.
- [30] E. Kometani and T. Sasaki. On the stability of traffic flow (report-i). *Journal of the Operations Research Society of Japan*, 2(1):11–26, 1958.
- [31] R. Korbmacher, P. Khound, and A. Tordeux. Understanding collective stability of ACC systems: From theory to real-world observations. *arXiv preprint arXiv:2504.04530*, 2025.
- [32] A. R. Kreidieh, C. Wu, and A. M. Bayen. Dissipating stop-and-go waves in closed and open networks via deep reinforcement learning. In *2018 21st international conference on intelligent transportation systems (itsc)*, pages 1475–1480. IEEE, 2018.
- [33] J. A. Laval, C. S. Toth, and Y. Zhou. A parsimonious model for the formation of oscillations in car-following models. *Transportation Research Part B: Methodological*, 70:228–238, 2014.

- [34] J. W. Lee, H. Wang, K. Jang, A. Hayat, M. Bunting, A. Alanqary, W. Barbour, Z. Fu, X. Gong, G. Gunter, et al. Traffic control via connected and automated vehicles: An open-road field experiment with 100 cavs. *arXiv preprint arXiv:2402.17043*, 2024.
- [35] T. Li, D. Chen, H. Zhou, J. Laval, and Y. Xie. Car-following behavior characteristics of adaptive cruise control vehicles based on empirical experiments. *Transportation research part B: methodological*, 147:67–91, 2021.
- [36] X. Li, J. Cui, S. An, and M. Parsafard. Stop-and-go traffic analysis: Theoretical properties, environmental impacts and oscillation mitigation. *Transportation Research Part B: Methodological*, 70:319–339, 2014.
- [37] M. J. Lighthill and G. B. Whitham. On kinematic waves ii. a theory of traffic flow on long crowded roads. *Proceedings of the Royal Society of London. Series A. Mathematical and Physical Sciences*, 229(1178):317–345, 1955.
- [38] M. Makridis, K. Mattas, A. Anesiadou, and B. Ciuffo. OpenACC. an open database of car-following experiments to study the properties of commercial ACC systems. *Transportation Research Part C: Emerging Technologies*, 125:103047, 2021.
- [39] M. Makridis, K. Mattas, and B. Ciuffo. Response time and time headway of an adaptive cruise control. an empirical characterization and potential impacts on road capacity. *IEEE Transactions on Intelligent Transportation Systems*, 21(4):1677–1686, 2019.
- [40] N. Maruyama and H. Mouri. A proposal for adaptive cruise control balancing followability and comfortability through reinforcement learning. *ROBOMECH Journal*, 9(1):22, 2022.
- [41] V. Milanés and S. E. Shladover. Modeling cooperative and autonomous adaptive cruise control dynamic responses using experimental data. *Transportation Research Part C: Emerging Technologies*, 48:285–300, 2014.
- [42] T. Nagatani. Modified KdV equation for jamming transition in the continuum models of traffic. *Physica A: Statistical Mechanics and its Applications*, 261(3-4):599–607, 1998.
- [43] G. F. Newell. Nonlinear effects in the dynamics of car following. *Operations Research*, 9(2):209–229, 1961.
- [44] G. F. Newell. A simplified car-following theory: a lower order model. *Transportation Research Part B: Methodological*, 36(3):195–205, 2002.
- [45] D. Ngoduy, S. Lee, M. Treiber, M. Keyvan-Ekbatani, and H. Vu. Langevin method for a continuous stochastic car-following model and its stability conditions. *Transportation Research Part C: Emerging Technologies*, 105:599–610, 2019.
- [46] G. Orosz, R. Wilson, and B. Krauskopf. Global bifurcation investigation of an optimal velocity traffic model with driver reaction time. *Physical Review E*, 70(2):026207, 2004.
- [47] G. Orosz, R. Wilson, and G. Stépán. Traffic jams: dynamics and control, 2010.
- [48] L. A. Pipes. An operational analysis of traffic dynamics. *Journal of Applied Physics*, 24(3):274–281, 1953.

- [49] A. Reuschel. Fahrzeugbewegungen in der Kolonne. *Österreichisches Ingenieur Archiv*, 4:193–215, 1950.
- [50] P. I. Richards. Shock waves on the highway. *Operations Research*, 4(1):42–51, 1956.
- [51] A. Schadschneider, D. Chowdhury, and K. Nishinari. *Stochastic Transport in Complex Systems. From Molecules to Vehicles*. Elsevier, 2010.
- [52] A. Schadschneider, D. Chowdhury, and K. Nishinari. *Stochastic transport in complex systems: from molecules to vehicles*. Elsevier, Amsterdam, 2011.
- [53] Y. Sugiyama, M. Fukui, M. Kikuchi, K. Hasebe, A. Nakayama, K. Nishinari, S.-i. Tadaki, and S. Yukawa. Traffic jams without bottlenecks—experimental evidence for the physical mechanism of the formation of a jam. *New Journal of Physics*., 10(3):033001, 2008.
- [54] E. Tomer, L. Safonov, and S. Havlin. Presence of many stable nonhomogeneous states in an inertial car-following model. *Physical Review Letters*, 84(2):382, 2000.
- [55] A. Tordeux, S. Lassarre, and M. Roussignol. An adaptive time gap car-following model. *Transportation Research Part B: Methodological*, 44(8-9):1115–1131, 2010.
- [56] A. Tordeux, M. Roussignol, and S. Lassarre. Linear stability analysis of first-order delayed car-following models on a ring. *Physical Review E*, 86(3):036207, 2012.
- [57] M. Treiber and D. Helbing. Hamilton-like statistics in onedimensional driven dissipative many-particle systems. *The European Physical Journal B*, 68:607–618, 2009.
- [58] M. Treiber, A. Hennecke, and D. Helbing. Congested traffic states in empirical observations and microscopic simulations. *Physical Review E*, 62(2):1805–1824, Aug. 2000.
- [59] M. Treiber and A. Kesting. Traffic flow dynamics. *Traffic Flow Dynamics: Data, Models and Simulation*, Springer-Verlag Berlin Heidelberg, pages 983–1000, 2013.
- [60] M. Treiber and A. Kesting. The intelligent driver model with stochasticity-new insights into traffic flow oscillations. *Transportation research procedia*, 23:174–187, 2017.
- [61] P. Wagner. A time-discrete harmonic oscillator model of human car-following. *The European Physical Journal B*, 84:713–718, 2011.
- [62] Y. Wang, X. Li, J. Tian, and R. Jiang. Stability analysis of stochastic linear car-following models. *Transportation Science*, 54(1):274–297, 2020.
- [63] U. Weidmann. Transporttechnik der Fußgänger: transporttechnische Eigenschaften des Fußgängerverkehrs. *IVT Schriftenreihe*, 90, 1993.
- [64] R. Wilson and J. Ward. Car-following models: Fifty years of linear stability analysis – a mathematical perspective. *Transportation Planning and Technology*, 34(1):3–18, 2011.
- [65] H. Winner, B. Danner, and J. Steinle. Adaptive cruise control. *Handbuch Fahrerassistenzsysteme: Grundlagen, Komponenten und Systeme für aktive Sicherheit und Komfort*, pages 478–521, 2009.
- [66] T. Xu and J. A. Laval. Analysis of a two-regime stochastic car-following model: Explaining capacity drop and oscillation instabilities. *Transportation Research Record*, 2673(10):610–619, 2019.